CEAS-GNC-2024-099

EuroGNC Navigation Guidance Control CEAS Bristol, UK June 11th-13th 2024
University of BRISTOL ROYAL AERONAUTICAL SOCIETY AIAA

A hybrid model for robust impulsive control applied to spacecraft rendezvous

Gianluca Napoletano Master's student in Space Engineering, Politecnico di Milano, Department of Aerospace Science and Technology, 20161, Milan, Italy. gianluca1.napoletano@mail.polimi.it

Alexandre Seuret Distinguished Researcher, Universidad de Sevilla, Department of Systems Engineering and Automation, 41092 Sevilla, Spain. aseuret@us.es

Rafael Vazquez Professor, Universidad de Sevilla, Department of Aerospace Engineering, 41092, Seville, Spain. rvazquez1@us.es

ABSTRACT

This work considers a hybrid systems framework to address the guidance problem for spacecraft rendezvous, under the assumptions of the Hill-Clohessy-Wiltshire model (target spacecraft in a circular Keplerian orbit). A feedback law is designed, based on a certain Lyapunov function and the solution of an Linear Matrix Inequality, which is then robustified against noise. A realistic model is used for simulations, with the dynamics of both chaser and target being propagated through a two-body problem model and including disturbances. The robust design shows enhanced control performance against noise when compared to its non-robust counterpart. In addition, a comparative analysis with Model Predictive Control (MPC), a popular method for spacecraft rendezvous, is conducted using the Monte Carlo method, highlighting the differences with the proposed controller, namely, simplicity and ease of computation versus optimality and implicit treatment of constraints.

Keywords: Spacecraft rendezvous; Spacecraft GNC; Hybrid systems; Impulsive control; LMIs

Nomenclature

n	=	mean motion
μ	=	Earth planetary constant
$\delta\mathbf{X}$	=	relative chaser state
$\delta\mathbf{r}$	=	relative chaser position
$\delta\mathbf{v}$	=	relative chaser velocity
$\mathbf{X}$	=	state (generic) expressed in Geocentric Equatorial frame
$\mathbf{u}$	=	impulsive control actuation
τ	=	timer of the hybrid control system
T	=	period between two impulsive manoeuvres
T_s	=	sampling time measurements
ϕ	=	pixel resolution of the optical tracking camera
$\delta\theta_\mathbf{c}$	=	measurement misalignment error

1 Introduction

The advent of intricate space missions has underscored the critical importance of satellite servicing operations, that rely on the precise maneuvering of an active spacecraft, referred to as the chaser, in the vicinity of another, known as the target. Such maneuvers, collectively termed rendezvous and proximity operations, necessitate guiding the follower to a designated area close to the leader before initiating the specific tasks required by the mission. The need for autonomous guidance and control for relative motion is paramount, enabling a plethora of space activities such as asteroid mining [1], collision avoidance [2], on-orbit assembly [3], satellite [4], and space station resupplying [5]. The initial impetus for proximity operations emerged from the Apollo program's innovative lunar orbital rendezvous concept [6], which aimed to reduce payload mass by separating the lunar and command modules upon entering the Moon's orbit. This technique was critical to the Apollo program's success and led to the development of the simplified Clohessy-Wiltshire equations [7], which provide a foundational understanding of the relative dynamics between two orbiting vehicles. The relevance of these operations has only grown, extending beyond the Apollo program to become a staple in low Earth orbit activities, as exemplified by the frequent rendezvous of various spacecraft with the International Space Station (ISS). However, the rapid expansion of space operations into new realms necessitates a continual evolution of spacecraft control strategies in proximity operations.

Our study focuses on the terminal phase of these operations, aiming to design efficient impulsive maneuvers that lead the chaser near the target. Historically, the planning phase of rendezvous missions often adopts the impulsive maneuver approximation, which simplifies the control and guidance design by assuming instantaneous velocity increments, a method widely acknowledged and utilized in rendezvous literature, thus justifying our impulsive approach. Employing a hybrid systems framework [8] grounded in the Hill-Clohessy-Wiltshire (HCW) model, we design a Lyapunov-based impulsive feedback control law for guaranteed stability computed through a Linear Matrix Inequality (LMI). The design is then extended to achieve robustness against disturbances. We demonstrate the adequate performance of our robust control law through simulations that employ a realistic model, accounting for disturbances in the two-body problem dynamics of both the chaser and the target spacecraft. Furthermore, we provide a comparative analysis with the Model Predictive Control (MPC) approach, a popular method in the rendezvous literature (see e.g. [9–12]) revealing our controller's advantages in simplicity and computational efficiency, in contrast to the MPC, which provides better optimality and constraint handling. It must be noted that there exist some precedent [13] in the use of hybrid systems to design impulsive control laws for rendezvous, which considered even more complex models than HCW, but compared with the work presented here, the authors did not use LMIs or a robust design against disturbances.

The manuscript is organized as follows. In Section 2 we introduce the HCW model used our work. We continue with Section 3 where the hybrid systems framework is introduced and our feedback control law designed. The simulation and disturbances model, simulation results and comparison with MPC are presented in Section 4. We conclude the paper with some closing remarks in Section 6.

2 Model of spacecraft rendezvous

In this work, we consider a passive and non-maneuvering target vehicle and a chaser vehicle which is active and performs the maneuvers to bring itself close to the target. The main assumptions to derive a dynamical model are that the target is in a Keplerian circular orbit, and the chaser is in close proximity to the target; neither target nor chaser are considered to be subject to orbital perturbations. Perturbations are not considered in this work. Then, the dynamics are described by the Hill-Clohessy-Wiltshire (HCW)

equations [14], given by

$$\delta\ddot{x} - 3n^2\delta x - 2n\delta\dot{y} = 0 \tag{1a}$$

$$\delta\ddot{y} + 2n\delta\dot{x} = 0 \tag{1b}$$

$$\delta\ddot{z} + n^2\delta z = 0 \tag{1c}$$

Here, δx, δy and δz denote the position of the chaser expressed in a local-vertical/local-horizontal (LVLH) frame of reference fixed on the target vehicle (See fig. 1), in which the x axis lies along the target position ($\mathbf{r}_0$), the y axis points in the direction of the local horizon, and z is perpendicular to the orbital plane of the target. The parameter n (the mean motion) is $n = \sqrt{\frac{\mu}{r_0^3}}$ (where μ is the gravitation parameter of the Earth, $\mu = 398600.4\ km^3/s^2$ and r_0 the radius of the target's orbit).

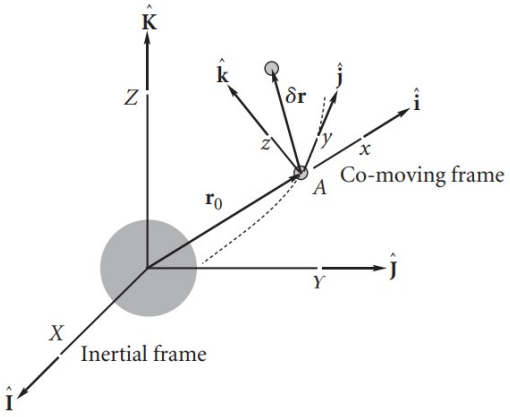

Fig. 1 Co-moving Clohessy-Wiltshire frame

The equations eq. (1) can be compactly written as

$$\delta\dot{\mathbf{X}} = \mathbf{A}\delta\mathbf{X} \tag{2}$$

where $\delta\mathbf{X} = \begin{bmatrix}\delta x & \delta y & \delta z & \delta\dot{x} & \delta\dot{y} & \delta\dot{z}\end{bmatrix}^\top$ and $\mathbf{A} = \begin{bmatrix} 0 & 0 & 0 & 1 & 0 & 0 \\ 0 & 0 & 0 & 0 & 1 & 0 \\ 0 & 0 & 0 & 0 & 0 & 1 \\ 3n^2 & 0 & 0 & 0 & 2n & 0 \\ 0 & 0 & 0 & -2n & 0 & 0 \\ 0 & 0 & -n^2 & 0 & 0 & 0 \end{bmatrix}$.

The impact of the control action can be accounted for by modeling it as an impulsive change in velocity. Denoting t^+ as the time instant when the instantaneous ΔV maneuver is executed

$$\delta\mathbf{X}^+ = \delta\mathbf{X}(t^+) = \delta\mathbf{X}(t) + \mathbf{B}\mathbf{u}(t) \tag{3}$$

where $\mathbf{u} = \begin{bmatrix}\Delta V_x & \Delta V_y & \Delta V_z\end{bmatrix}^T$ is the impulsive control actuation and $\mathbf{B} = \begin{bmatrix} 0_{3\times3} \\ I_3 \end{bmatrix}$, meaning that after applying an instantaneous ΔV change, the chaser will have the same relative position but different relative velocity with respect to the target. This analysis reveals that the model exhibits both continuous and discrete dynamics, and can be formulated as a hybrid dynamical system.

3 An LMI-based control design for impulsive systems

The aim of this section is to formulate a robust control strategy for the precise execution of the rendezvous operation. This begins with a concise exposition of the theory pertaining to hybrid dynamical systems [8, 15], and their customization to our specific case scenario. This customization process aligns

with prior investigations [13, 16] on hybrid systems as applied to spacecraft rendezvous scenarios. Lastly, some modifications to design a more robust controller will be considered.

3.1 Hybrid dynamical systems

The maneuver executed by the chaser can be approximated as an instantaneous alteration in velocity, denoted as ΔV. Consequently, the underlying dynamical system can be regarded as a hybrid system. The latter encompasses characteristics of both continuous and discrete dynamics, allowing for continuous flow and abrupt transitions. In essence, it signifies a system that can both evolve continuously and undergo discrete jumps. This type of systems can be generally formalized as follows:

$$\mathcal{H} = (C, \mathcal{D}, F, G) \tag{4}$$

where $n_x \in \mathbb{N}$ is the state dimension, $C \subseteq \mathbb{R}^{n_x}$ is the flow set, $\mathcal{D} \subseteq \mathbb{R}^{n_x}$ is the jump set, $F : C \rightrightarrows \mathbb{R}^{n_x}$ is the flow map and $G : \mathcal{D} \rightrightarrows \mathbb{R}^{n_x}$ the jump map. Mathematically, $\mathcal{H}$ is given by

$$\mathcal{H} : \begin{cases} \dot{x} \in F(x), & x \in C \quad (5a) \\ x^+ \in G(x), & x \in \mathcal{D} \quad (5b) \end{cases}$$

A solution of $\mathcal{H}$ can experience a continuous or a discrete evolution depending the current value of x. For instance, if the jump (or flow) set is empty, the hybrid system refers to a usual continuous-time differential systems (discrete-time systems). The Hybrid dynamical systems offers the possibility to consider both approach simultaneously. In the context of the HCW model (2), it is possible to express the flow equation that captures the continuous dynamical behaviour of the system as follows

$$\delta\dot{\mathbf{X}} = \mathbf{A}\delta\mathbf{X}, \quad \text{when there is no impulses.} \tag{6}$$

The jumps refers to the equation eq. (3), which allows for a seamless transition between the continuous and discrete dynamics of the system. This equation encapsulates the instantaneous changes induced by the maneuver, ensuring the integration of both continuous and discrete elements within the overall system behavior.

$$\delta\mathbf{X}^+ = \begin{bmatrix} \delta\mathbf{r}^+ \\ \delta\mathbf{v}^+ \end{bmatrix} = \begin{bmatrix} \delta\mathbf{r} \\ \delta\mathbf{v} + \mathbf{u} \end{bmatrix}, \quad \text{when an impulse occurs.} \tag{7}$$

As previously pointed out, the position remains constant across jumps, while the velocity undergoes a modification by incorporating a factor denoted as $\mathbf{u}$, which represents the impulsive control actuation.

It remains to characterized the jump and flow sets associated to this system to characterized when impulses are allowed. In this paper, we will enforce jumps at periodic instants of time, with a given and known period denoted as $T > 0$. To do so and to provide a complete hybrid model of the HCW model with periodic impulse, it is necessary to include a timer that account for the time elapsed since the last impulse. This is formulated as follows:

$$\begin{cases} \delta\dot{\mathbf{X}} = \mathbf{A}\delta\mathbf{X} \\ \dot{\tau} = 1 \end{cases} \quad (\delta\mathbf{X}, \tau) \in C := \{(\xi, \xi_\tau) \in \mathbb{R}^7,\ \xi_\tau \leq T\}$$
$$\begin{cases} \delta\mathbf{X}^+ = \delta\mathbf{X} + \mathbf{B}\mathbf{u} \\ \tau^+ = 0 \end{cases} \quad (\delta\mathbf{X}, \tau) \in C := \{(\xi, \xi_\tau) \in \mathbb{R}^7,\ \xi_\tau = T\} \tag{8}$$

The variable τ works as a timer. This means that when the system starts propagating in continuous time (flow map), the timer is activated and begins counting upwards. Once it reaches a prefixed value of the sampling period T, that in our case will represent the time interval between one impulsive manoeuvre and

another one, the system undergoes a discrete jump wherein the velocity is modified while the position remains unchanged. Subsequently, the timer is reset to 0, and the system resumes continuous-time propagation.

The objective of the paper is to design a state feedback control law

$$\mathbf{u} = \mathbf{K}\delta\mathbf{X} \tag{9}$$

for a given gain $\mathbf{K}$ in $\mathbb{R}^{3\times 6}$ such that the set $\mathcal{A} = \left\{(\xi, \xi_\tau) \in \mathbb{R}^7, \xi = 0 \text{ and } \xi_\tau \in [0, T]\right\}$ is an attractor for the closed-loop system (8),(9), i.e. that the state of the hybrid system $(\delta\mathbf{X}, \tau)$ converges asymptotically to the set defined by $\delta\mathbf{X} = 0$ and $\tau \in [0, T]$.

3.2 Extension of Lyapunov theorem for hybrid systems

In this context, we introduce an extension of the Lyapunov theorem tailored for hybrid systems. This extension allows us to leverage the theorem's principles to identify a suitable candidate Lyapunov function, which serves as a foundation for deriving the control logic. By employing this approach, we can systematically analyze the stability and convergence properties of the hybrid system, facilitating the design of effective control strategies.

Theorem 3.1 (Lyapunov Theorem)**.** *Given a hybrid dynamical system*

$$\mathcal{H}: \begin{cases} \dot{x} \in F(x), & x \in \mathcal{C} \quad (10a) \\ x^+ \in G(x), & x \in \mathcal{D} \quad (10b) \end{cases}$$

assume that the function $V : \mathbb{R} \to \mathbb{R}_{\geq 0}$ satisfies for some positive scalars c_1, c_2 and c_3:

$$c_1|x|_{\mathcal{A}}^2 \leq V(x) \leq c_2|x|_{\mathcal{A}}^2, \qquad \forall x \in \mathcal{C} \cup \mathcal{D} \cup G(\mathcal{D}) \tag{11}$$

$$\langle \nabla V, f(x) \rangle \leq -c_3|x|_{\mathcal{A}}^2, \qquad \forall x \in \mathcal{C} \tag{12}$$

$$V(g(x)) - V(x) \leq -c_3|x|_{\mathcal{A}}^2, \qquad \forall x \in \mathcal{D} \tag{13}$$

then the origin is uniformly globally exponentially stable.

In the previous theorem, notation $|\cdot|_{\mathcal{A}}$ stands for the distance of x to the attractor. The previous theorem means that we want to build a positive definite function of the state, which decreases both during flows and jumps.

3.3 Stabilization of the HCW model with periodic impulses

Based on the hybrid formulation of the HCW model (8) with the control law (9), the following theorem presents a stabilization condition of the hybrid closed-loop system that is expressed in terms of an Linear Matrix Inequality (LMI). Before stating the first theorem of this paper, a brief introduction of the necessary notations to understand the LMI framework. A symmetric positive definite matrix W is said positive definite if all its eigenvalues are strictly positive. As it is well-known that symmetric matrices have only real eigenvalues, it is possible to introduce a relation of order for symmetric matrices. In particular, we will use the notations $W \succ 0$ and $W \prec 0$ to denote that matrix W is symmetric positive definite and symmetric negative definite. In addition, for any matrices $A = A^\top$, B and $C = C^\top$ of appropriate dimensions, notation $\left[\begin{smallmatrix} A & B \\ * & C \end{smallmatrix}\right]$ stands for the symmetric matrix $\left[\begin{smallmatrix} A & B \\ B^\top & C \end{smallmatrix}\right]$.

We are now in position to state the first result of the paper

Theorem 3.2. *Assume that there exist a* 6×6*-symmetric positive definite matrix* $\mathbf{W} \succ 0$ *and a* 3×6*-matrix* $\mathbf{Y}$ *such that*

$$\begin{bmatrix} -\mathbf{W} & \mathbf{W} + \mathbf{Y}^\top \mathbf{B}^\top e^{A^\top T} \\ * & -\mathbf{W} \end{bmatrix} \prec 0. \tag{14}$$

Then, the control gain $\mathbf{K} = \mathbf{Y}\mathbf{W}^{-1}$ *under the periodic impulses of period* T *stabilizes hybrid closed-loop system* (8),(9) *to the attractor* $\mathcal{A}$.

Proof. Consider the hybrid model of the closed-loop system eq. (15),(9) with a gain $\mathbf{K}$ to be defined. The closed-loop system writes as follows

$$\begin{cases} \delta\dot{\mathbf{X}} &= \mathbf{A}\delta\mathbf{X} \\ \dot{\tau} &= 1 \end{cases} \quad (\delta\mathbf{X}, \tau) \in C, \qquad \begin{cases} \delta\mathbf{X}^+ &= \delta\mathbf{X} + \mathbf{B}\mathbf{K}\delta\mathbf{X} \\ \tau^+ &= 0 \end{cases} \quad (\delta\mathbf{X}, \tau) \in \mathcal{D}. \tag{15}$$

Indeed, re-injecting the expression of $\mathbf{u} = \mathbf{K}\delta\mathbf{X}$ in (8), the eq. (7) can be rewritten as $\delta\mathbf{X}^+ = \delta\mathbf{X} + \mathbf{B}\mathbf{K}\delta\mathbf{X}$. Consider the candidate Lyapunov function given by

$$V(\delta\mathbf{X}, \tau) = \delta\mathbf{X}^\top e^{-\mathbf{A}^\top \tau} \mathbf{P} e^{-\mathbf{A}\tau} \delta\mathbf{X} \tag{16}$$

where $\mathbf{P}$ is a positive definite matrix. As $\mathbf{P}$ is positive definite and since τ is bounded in $[0, T]$, it is clear the the first condition of the Lyapunov theorem (11) is verified.

Let us now compute the derivative of the Lyapunov function during flows, which gives

$$\dot{V}(\delta\mathbf{X}, \tau) = \delta\dot{\mathbf{X}}^\top e^{-\mathbf{A}^\top \tau} P e^{-\mathbf{A}\tau} \delta\mathbf{X} + \delta\mathbf{X}^\top e^{-\mathbf{A}^\top \tau} P e^{-\mathbf{A}\tau} \delta\dot{\mathbf{X}} - \delta\mathbf{X} e^{-\mathbf{A}^\top \tau} (\mathbf{A}^\top P + P\mathbf{A}) e^{-\mathbf{A}\tau} \delta\mathbf{X} = 0. \tag{17}$$

The previous inequality ensures that the second condition of the Lyapunov theorem (12) is fulfilled.

Let us now compute the variation of the Lyapunov function across jumps. Condition (13) requires that, at each jump, the difference between V after and before jumps is negative. To do so, let us note that, in the jump set , timer τ is necessarily equal to T and that after a jump the timer τ is reset to 0. Hence, we obtain:

$$V(\delta\mathbf{X}, \tau = T) = \delta\mathbf{X}^\top e^{-\mathbf{A}^\top T} \mathbf{P} e^{-\mathbf{A}T} \delta\mathbf{X}, \quad V(\delta\mathbf{X}^+, \tau^+) = \delta\mathbf{X}^{+\top} \mathbf{P} \delta\mathbf{X}^+. \tag{18}$$

It is now possible to retrieve the equation reported hereafter.

$$\begin{aligned} \Delta V(\delta\mathbf{X}, \tau) &= V(\delta\mathbf{X}^+, \tau^+) - V(\delta\mathbf{X}, \tau) = V((\mathbf{I} + \mathbf{B}\mathbf{K})\delta\mathbf{X}, 0) - V(\delta\mathbf{X}, T) \\ &= \delta\mathbf{X}^\top (\mathbf{I} + \mathbf{B}\mathbf{K})^\top \mathbf{P} (\mathbf{I} + \mathbf{B}\mathbf{K}) \delta\mathbf{X} - \delta\mathbf{X}^\top e^{-\mathbf{A}^\top T} P e^{-\mathbf{A}T} \delta\mathbf{X} \\ &= \delta\mathbf{X}^\top ((\mathbf{I} + \mathbf{B}\mathbf{K})^\top \mathbf{P} (\mathbf{I} + \mathbf{B}\mathbf{K}) - e^{-\mathbf{A}^\top \tau} \mathbf{P} e^{-\mathbf{A}\tau}) \delta\mathbf{X} \end{aligned} \tag{19}$$

Defining $\mathbf{Q} = e^{-\mathbf{A}^\top T} \mathbf{P} e^{-\mathbf{A}T}$, eq. (19) is rewritten as :

$$\Delta V(\delta\mathbf{X}, \tau) = \delta\mathbf{X}^\top ((\mathbf{I} + \mathbf{B}\mathbf{K})^\top e^{\mathbf{A}^\top T} \mathbf{Q} e^{\mathbf{A}T} (\mathbf{I} + \mathbf{B}\mathbf{K}) - \mathbf{Q}) \delta\mathbf{X} = \delta\mathbf{X}^\top \Pi \delta\mathbf{X}, \tag{20}$$

with $\Pi = (\mathbf{I}+\mathbf{B}\mathbf{K})^\top e^{\mathbf{A}^\top T} \mathbf{Q} e^{\mathbf{A}T} (\mathbf{I}+\mathbf{B}\mathbf{K}) - \mathbf{Q}$. Then, ΔV is negative across jumps if and only if matrix Π is symmetrix negative definite, which can be stated as a matrix inequality. However this condition is not an LMI (linear) since the matrix Π is defined as a nonlinear expression of the unknown decision variables

Q and K. Hence matrix Π needs to be linearized in order to retrieve the values of $\mathbf{K}$ and $\mathbf{Q}$ such that the term Π is symmetric negative definite.

To do so, we exploit the so-called Schur complement, which provides an equivalent formulation of inequality $\Pi < 0$, which writes

$$\Pi \prec 0 \Leftrightarrow \begin{bmatrix} -\mathbf{Q} & (\mathbf{I}+\mathbf{B}\mathbf{K})^\top e^{\mathbf{A}^\top T} \\ * & -\mathbf{Q}^{-1} \end{bmatrix} \prec 0 \tag{21}$$

Now using a congruence, that means that for any non singular matrix M, condition $\Pi < 0$ is equivalent to $M^\top \Pi M \prec 0$. In particular, selecting $\mathbf{M} = \begin{bmatrix} \mathbf{Q}^{-1} & \mathbf{0} \\ * & \mathbf{I} \end{bmatrix}$ yields

$$\Pi \prec 0 \Leftrightarrow \begin{bmatrix} -\mathbf{Q}^{-1} & \mathbf{Q}^{-1}(\mathbf{I}+\mathbf{B}\mathbf{K})^\top e^{\mathbf{A}^\top T} \\ * & -\mathbf{Q}^{-1} \end{bmatrix} \prec 0 \tag{22}$$

The LMI condition is then obtained by selecting $\mathbf{Q} = \mathbf{W}^{-1}$ and $\mathbf{K} = \mathbf{Y}\mathbf{W}^{-1}$: This means that if condition (14) holds, then matrix Π is symmetric negative definite.

The proof is then concluded by noting that the system enter periodically into the jump set, which ensures a regular decrease of the Lyapunov function, even though during flows, the Lyapunov function is constant. □

It is crucial to note that this procedure is carried out offline, eliminating the need to solve an optimization problem at each time instant in which the control has to be applied, as required in the case of MPC (Model Predictive Control) techniques. This distinction is significant, particularly when considering limited computational resources, as it enhances computational efficiency and expedites the process.

3.4 Robustness of the control law with respect to exogenous noise

The control law designed in the previous section requires the exact measure of the state of the system, i.e. the relative positions and velocities. However, in practice, measuring the exact value of the current positions and velocities is not an easy tasks because their measurement is performed using an optical tracking camera on board, which induces measurement noise. Therefore, the propagation of this noise in the control action has to be considered with attention.

To consider this issue, we will first propose a model that accounts for the bounded measurement noise. The following assumption is made

Assumption 3.1. *The output measure of the state is given by*

$$\delta\hat{\mathbf{X}} := \delta\mathbf{X} + d \tag{23}$$

where d in $\mathbb{R}^6$ stands for the noise vector, which is such that there exists $\bar{d}$ in $\mathbb{R}$ so that the following inequality holds

$$d \in \Omega_d := \{v \in \mathbb{R}^6, \ \ s.t.\ v^\top v \leq \bar{d}^2\}. \tag{24}$$

We now may rewrite the hybrid dynamical system as follows

$$\begin{cases} \delta\dot{\mathbf{X}} &= \mathbf{A}\delta\mathbf{X} \\ \dot{\tau} &= 1 \\ \dot{d} &= 0 \end{cases} \qquad (\delta\mathbf{X}, \tau, d) \in C_d := \{(\xi, \xi_\tau, \xi_d) \in \mathbb{R}^{13},\ \text{s.t}\ \xi_\tau \leq T \text{ and } \xi_d \in \Omega_d\},$$

$$\begin{cases} \delta\mathbf{X}^+ &= \delta\mathbf{X} + \mathbf{BK}\delta\mathbf{X} + \mathbf{BK}d \\ \tau^+ &= 0 \\ d^+ &\in \Omega_d \end{cases} \qquad (\delta\mathbf{X}, \tau, d) \in \mathcal{D}_d := \{(\xi, \xi_\tau, \xi_d) \in \mathbb{R}^{13}\ \text{s.t}\ \xi_\tau = T \text{ and } \xi_d \in \Omega_d\}. \tag{25}$$

The objective is now to ensure that the closed loop system converges to the following attractor

$$\mathcal{A}_d := \{(\xi, \xi_d) \in \mathbb{R}^7 \times \mathbb{R}^6\ \text{s.t}\ V(\xi) \leq 1,\ \xi_\tau \in [0, T] \text{ and } \xi_d \in \Omega_d\}, \tag{26}$$

where V is the Lyapunov function to be designed.

Before stating the theorem of this section, let us introduce the following lemma (S-Procedure [17]) that will be useful in the next developments

Lemma 3.3 (S-procedure)**.** *For given symmetric matrices M and N of appropriate dimension, the following statements are equivalent*

- $X^\top M X < 0\ \forall X\ s.t\ X^\top N X > 0$
- $\exists \eta > 0\ s.t\ M - \eta N \prec 0$

We are now in position to state the next theorem.

Theorem 3.4. *For given $\eta > 0$ and $\epsilon > 0$ and $\bar{d} \geq 0$, assume that there exist a symmetric positive definite matrix $\mathbf{W} > 0$ and a matrix $\mathbf{Y}$ such that*

$$\begin{bmatrix} -(1-\eta)\mathbf{W} & \mathbf{0} & \mathbf{W}\mathbf{F}^\top + \mathbf{Y}^\top\mathbf{B}^\top\mathbf{F}^\top \\ * & -\frac{\eta}{\bar{d}^2}(2\epsilon\mathbf{W} - \epsilon^2\mathbf{I}) & \mathbf{Y}^\top\mathbf{B}^\top\mathbf{F}^\top \\ * & * & -\mathbf{W} \end{bmatrix} \prec 0 \tag{27}$$

Then the control gain $\mathbf{K} = \mathbf{Y}\mathbf{W}^{-1}$ stabilizes hybrid system (25)*, that includes the the bounded measurement noise and the periodic impulses policy of period T, to the attractor $\mathcal{A}_d$, which corresponds to a bounded region of the state space such that $V(\delta X, \tau) < 1$ around $\delta\mathbf{X} = 0$.*

Proof. Consider the same Lyapunov function as in the previous section and given in (16). Following the same procedure as in the previous proof of the previous theorem, this function is positive definite and is constant during flows. Indeed, this is due to the fact that the measurement noise only affects the jump map and not the flow map.

Let us now compute the variation of the Lyapunov function across jumps. For the sake of simplicity, we introduce notation $\mathbf{F} = e^{-\mathbf{A}^\top T}$ to ease the reading of the next developments. The new expression of ΔV is then given by

$$\begin{aligned} \Delta V(\delta\mathbf{X}, \tau) &= V(\delta\mathbf{X}^+, \tau^+) - V(\delta\mathbf{X}, \tau) \\ &= ((\mathbf{I} + \mathbf{BK})\delta\mathbf{X} + \mathbf{BK}d)^\top\mathbf{P}((\mathbf{I} + \mathbf{BK})\delta\mathbf{X} + \mathbf{BK}d) - \delta\mathbf{X}^\top\mathbf{F}^\top\mathbf{P}\mathbf{F}\delta\mathbf{X} \\ &= ((\mathbf{I} + \mathbf{BK})\delta\mathbf{X} + \mathbf{BK}d)^\top\mathbf{F}^\top\mathbf{Q}\mathbf{F}((\mathbf{I} + \mathbf{BK})\delta\mathbf{X} + \mathbf{BK}d)^\top - \delta\mathbf{X}^\top\mathbf{Q}\delta\mathbf{X}, \end{aligned} \tag{28}$$

where we recall notation $\mathbf{Q} = e^{-\mathbf{A}^\top T}\mathbf{P}e^{-\mathbf{A}T}$. This expression can be rearranged in the following quadratic form.

$$\Delta V(\delta\mathbf{X}, \tau) = \begin{bmatrix} \delta\mathbf{X} \\ d \end{bmatrix}^\top \Delta \begin{bmatrix} \delta\mathbf{X} \\ d \end{bmatrix} \tag{29}$$

where

$$\Delta = \begin{bmatrix} \mathbf{I} + \mathbf{BK} & \mathbf{BK} \end{bmatrix}^\top \mathbf{F}^\top \mathbf{Q}\mathbf{F} \begin{bmatrix} \mathbf{I} + \mathbf{BK} & \mathbf{BK} \end{bmatrix} - \begin{bmatrix} \mathbf{Q} & \mathbf{0} \\ \mathbf{0} & \mathbf{0} \end{bmatrix}. \tag{30}$$

The main idea is that when the chaser is far from the target, the components of the relative state $\delta\mathbf{X}$ (position and velocity) are large. As a result, the noise has a minor impact on the system. On the contrary, as the chaser gets closer of the target, the relative state components decrease and the effect of the noise becomes more significant.

Let us note that outside of the attractor $\mathcal{A}_d$, the Lyapunov function is greater than 1 and the measurements noise verifies $d^\top d \leq \bar{d}^2$. Hence, we have

$$d^\top d \leq \bar{d}^2 \leq \bar{d}^2 \delta\mathbf{X}^\top \mathbf{Q} \delta\mathbf{X}, \quad \forall (\delta\mathbf{X}, \tau, d) \in \mathcal{D}_d \setminus \mathcal{A}_d. \tag{31}$$

The previous inequality can be rewritten in a quadratic form as follows

$$\begin{bmatrix} \delta\mathbf{X} \\ d \end{bmatrix}^\top \begin{bmatrix} \mathbf{Q} & \mathbf{0} \\ \mathbf{0} & -\frac{1}{\bar{d}^2}\mathbf{I} \end{bmatrix} \begin{bmatrix} \delta\mathbf{X} \\ d \end{bmatrix} \geq 0, \Leftrightarrow (\delta\mathbf{X}, \tau, d) \in \mathcal{D}_d \setminus \mathcal{A}_d. \tag{32}$$

To sum up, we want to guarantee that the Lyapunov function is decreasing across jump, i.e. when $(\delta\mathbf{X}, \tau, d) \in \mathcal{D}_d \setminus \mathcal{A}_d$, which writes

$$\begin{bmatrix} \delta\mathbf{X} \\ d \end{bmatrix}^\top \Delta \begin{bmatrix} \delta\mathbf{X} \\ d \end{bmatrix} \leq 0 \quad \forall (\delta\mathbf{X}, \tau, d) \text{ s.t } \begin{bmatrix} \delta\mathbf{X} \\ d \end{bmatrix}^\top \begin{bmatrix} \mathbf{Q} & \mathbf{0} \\ \mathbf{0} & -\frac{1}{\bar{d}^2}\mathbf{I} \end{bmatrix} \begin{bmatrix} \delta\mathbf{X} \\ d \end{bmatrix} \geq 0$$

This problem corresponds exactly to the formulation of the S-procedure in Lemma 3.3 by selecting

$$X = \begin{bmatrix} \delta\mathbf{X} \\ d \end{bmatrix}, \quad M = \begin{bmatrix} \mathbf{I} + \mathbf{BK} & \mathbf{BK} \end{bmatrix}^\top \mathbf{F}^\top \mathbf{Q}\mathbf{F} \begin{bmatrix} \mathbf{I} + \mathbf{BK} & \mathbf{BK} \end{bmatrix} - \begin{bmatrix} \mathbf{Q} & \mathbf{0} \\ \mathbf{0} & \mathbf{0} \end{bmatrix}, \quad N = \begin{bmatrix} \mathbf{Q} & \mathbf{0} \\ \mathbf{0} & -\frac{1}{\bar{d}^2}\mathbf{I} \end{bmatrix}. \tag{33}$$

Hence, applying Lemma 3.3, this previous problem is equivalent to the existence of a positive scalar $\eta \geq 0$ such that

$$\begin{bmatrix} -(1-\eta)\mathbf{Q} & \mathbf{0} & (\mathbf{I} + \mathbf{BK})^\top \mathbf{F}^\top \\ \mathbf{0} & -\eta\frac{1}{\bar{d}^2}\mathbf{I} & (\mathbf{BK})^\top \mathbf{F}^\top \\ \mathbf{0} & \mathbf{0} & -\mathbf{Q}^{-1} \end{bmatrix} \prec 0, \tag{34}$$

where we have used the Schur Complement to the first term of M. Exploiting again the congruence by pre- and post-multiplying the previous expression by $\mathbf{M} = \begin{bmatrix} \mathbf{W} & \mathbf{0} & \mathbf{0} \\ \mathbf{0} & \mathbf{W} & \mathbf{0} \\ \mathbf{0} & \mathbf{0} & \mathbf{I} \end{bmatrix}$ and its transpose respectively, where

$\mathbf{W} = \mathbf{Q}^{-1}$, we obtain

$$\begin{aligned} M - \eta N \prec 0 \quad &\Leftrightarrow \quad \mathbf{M}^\top \begin{bmatrix} -(1-\eta)\mathbf{Q} & \mathbf{0} & (\mathbf{I}+\mathbf{B}\mathbf{K})^\top \mathbf{F}^\top \\ * & -\frac{\eta}{\bar{d}^2}\mathbf{I} & (\mathbf{B}\mathbf{K})^\top \mathbf{F}^\top \\ * & * & -\mathbf{Q}^{-1} \end{bmatrix} \mathbf{M} \prec 0 \\ &\Leftrightarrow \quad \begin{bmatrix} -(1-\eta)\mathbf{W}\mathbf{Q}\mathbf{W} & \mathbf{0} & (\mathbf{W}+\mathbf{W}\mathbf{K}^\top \mathbf{B}^\top)\mathbf{F}^\top \\ * & -\frac{\eta}{\bar{d}^2}\mathbf{W}^2 & \mathbf{W}\mathbf{K}^\top \mathbf{B}^\top \\ * & * & -\mathbf{Q}^{-1} \end{bmatrix} \prec 0. \end{aligned} \tag{35}$$

As for the previous theorem, we introduce notations $\mathbf{W} = \mathbf{Q}^{-1}$ and $\mathbf{Y} = \mathbf{K}\mathbf{W}$ to get

$$M - \eta N \prec 0 \quad \Leftrightarrow \quad \begin{bmatrix} -(1-\eta)\mathbf{W} & \mathbf{0} & \mathbf{W}\mathbf{F}^\top + \mathbf{Y}^\top \mathbf{B}^\top \mathbf{F}^\top \\ * & -\frac{\eta}{\bar{d}^2}\mathbf{W}^2 & \mathbf{Y}^\top \mathbf{B}^\top \mathbf{F}^\top \\ * & * & -\mathbf{W} \end{bmatrix} \prec 0. \tag{36}$$

The previous expression is not an LMI because of the term $\frac{\eta}{\bar{d}^2}\mathbf{W}\mathbf{W}$, which is quadratic in the decision variable $\mathbf{W}$. To make it linear, we note that the quantity $(\epsilon\mathbf{I} - W)^2$ is positive definite. Expanding this expression and re-arranging the terms, we get that

$$\mathbf{W}^2 \succ 2\epsilon\mathbf{W} - \epsilon^2\mathbf{I}.$$

Injecting this inequality in (36) yeilds the stabilization condition of Theorem 3.4, which concludes the proof. □

The terms η and ϵ can be used as tuning parameters to modify the controller performance.

It is also worth noticing that when $\bar{d}$ tends to 0 (no noise), the previous stabilization condition tends to the condition of the first theorem (noise-free case), showing the continuity of the condition when the bound on the measurement noise tends to 0.

4 Simulations results

4.1 Rendezvous model

For the purpose of simulation, a more realistic model than HCW is used. First, the non linear two-body problem [14] is exploited to propagate the dynamics of both chaser and target spacecraft between one impulsive velocity change and another one, so that nonlinear effects are not neglected. The equation is the following:

$$\ddot{\mathbf{r}} = -\mu\frac{\mathbf{r}}{r^3}, \tag{37}$$

where the term $\mathbf{r}$ is the position vector of the spacecraft expressed in the Geocentric Equatorial frame. The overall system is modeled as displayed in fig. 2.

The terms $\mathbf{X}_C$ and $\mathbf{X}_T$ are 6-by-1 vectors containing position and velocity of chaser and target expressed in the inertial reference frame. Dealing with the model parameters, it is considered that both spacecraft are positioned in the same circular orbit at 500 km of altitude, meaning that $\mathbf{r}_0 = 6871$ km and $n = 1.1085 \times 10^{-3}$ rad/s. Regarding the actuator, the maximum ΔV change applicable is ± 0.2 m/s, and the minimum impulse bit (expressed as a variation in velocity) is 5 mm/s. The operation is concluded when the conditions 5 m $< \delta\mathbf{r} <$ 25 m and $\delta\mathbf{v} <$ 0.2 m/s are both satisfied.

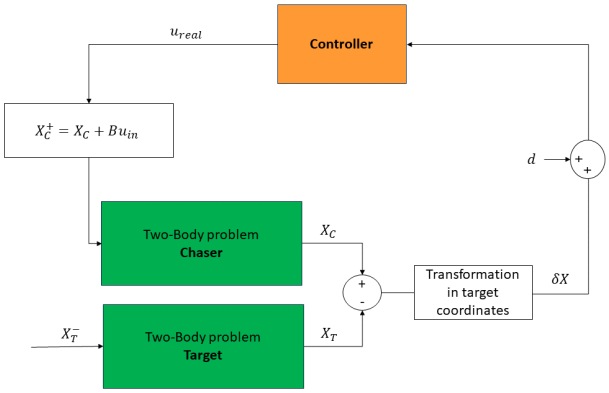

Fig. 2 System scheme: the two-body problem model is used to propagate both chaser and target dynamics, allowing to retrieve the relative state δX of the HCW model. The control input is then used to compute the new state of the chaser, which is fed as initial condition for the new integration step.

4.2 Disturbances model

A source of process noise is taken into account introducing the random variable **d**. To further incorporate disturbances in the control action, the actual applied thrust is modeled as follows:

$$\mathbf{u}_{real} = \mathbf{\Psi}(\delta\theta)(\mathbf{u} + \delta + b) \tag{38}$$

where **u** is the output commanded by the control laws, **b** is the bias, δ is a random variable, and $\mathbf{\Psi}(\delta\theta)$ denotes a rotation matrix where $\delta\theta$ is a vector of small, random angles modeling imperfect alignment. These disturbances model several physical aspects. First, the attitude control of the chaser is not perfect, so one can expect that the thrust generated by the actuators is not perfectly aligned with the intended direction; this is modeled by $\mathbf{\Psi}(\delta\theta)$. On the other hand, with δ one can model thrust disturbances. The term $\mathbf{u}_{in}$ displayed in fig. 2 represents the control input expressed in the Geocentric Equatorial frame.

4.3 Comparison of robust vs non-robust hybrid control law

The non-robust and robust controller introduced in section 3 are now compared. In this first analysis the constraints on the final position and velocity are not considered, together with the actuators saturation, and the simulation time is set to 2000 s. In fig. 3 (left), the non-robust controller is tested in two scenarios: a first ideal case in which the disturbances affecting the state and the actuators do not exist, and another one in which they are present. In the first ideal case (solid blue line), the non-robust controller reaches the target at the origin of the reference frame, completing the operation by bringing to zero both relative position and velocity of the chaser. Conversely, in the presence of disturbances, the control displays highly aggressive behavior, resulting in the chaser spacecraft oscillating around the target position due to significant velocity adjustments (dashed red line).

Next, the robust controller is tested on the same scenarios as showcased before, and the results are displayed in fig. 3 (right). It is evident that the robust controller demonstrates enhanced robustness against noise effects, as seen in its ability to safely reach the target position.

4.4 Comparison of hybrid control law with MPC

In this section, a comparative analysis between the LMI controller and a basic Model Predictive Control (MPC) design is conducted. The latter is a strategy commonly employed and extensively studied in spacecraft rendezvous operations [9, 18]. MPC is an optimal control technique in which the control

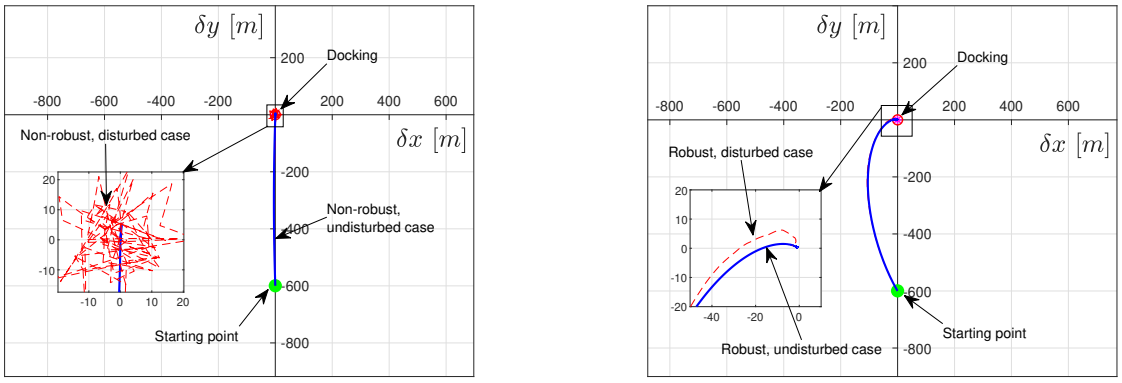

Fig. 3 Left: Non-robust control without disturbances (solid line) and with disturbances (dashed line). Right: Robust controller without disturbances (solid line) and with disturbances (dashed line). For both cases, d: $\bar{\mathbf{d}} = 0$, $\sqrt{\Sigma_{11,22,33}} = 10$, $\sqrt{\Sigma_{44,55,66}} = 1 \times 10^{-2}$; $\delta\theta$: $\delta\bar{\theta}_i = 0$,$\sqrt{\Sigma_{ii}} = 3.3 \times 10^{-4}$; δ: $\bar{\delta} = 0$,$\sqrt{\Sigma_{ii}} = 1 \times 10^{-3}$, $T = 30\ s$

action minimizes a cost function while satisfying a set of constraints over a finite receding horizon. The appropriate cost function and constraints for this scenario are depicted below:

$$J_k(\mathbf{x}_k, \mathbf{u_S}(k)) = \sum_{j=1}^{N_p} (\|\mathbf{x}_{k+j} - \mathbf{x}_t\|^2_{\mathbf{Q}} + \|\mathbf{u}_{k+j-1}\|^2_{\mathbf{R}}) + \|\mathbf{x}_{k+N_p} - \mathbf{x}_t\|^2_{\mathbf{P}} \tag{39}$$

$$\mathbf{u}_{min} \leq \mathbf{u_S}(k) \leq \mathbf{u}_{max} \tag{40}$$

where $\mathbf{u_S}$ is a set of N_p future control action, N_p is the length of the prediction horizon, $\mathbf{x}_t$ is the target state, and $\|\mathbf{x}\|_{\mathbf{A}} = \sqrt{\mathbf{x}^T\mathbf{A}\mathbf{x}}$. Due to the presence of random variables with normal distribution of probability (see section 4.2), a Monte Carlo analysis is conducted to compare the two controllers, considering a number of 100 simulations for each (see fig. 4). The current analysis considers the same disturbances and parameters as in the previous study, while also accounting for constraints on the control action, as well as the final relative position and velocity. To assess and compare performance, it is crucial to examine the total ΔV consumption in relation to the total time required to rendezvous with the target spacecraft. These metrics are displayed in fig. 5 (left), while the cumulative mean and standard deviation are outlined in fig. 5 (right).

Both controllers demonstrate comparable behaviors, exhibiting similar consumption in relation to the total time required to complete the operation. The main advantages of the LMI technique are twofold: first, the computation of the control gain matrix is performed offline, eliminating the necessity to solve multiple optimization problems during the maneuver; second, it possesses the ability to ensure stability, a feat that proves to be a challenge for MPC to match. Conversely, one of the primary strengths of the MPC controller is its capability to satisfy a range of constraints. One of the most crucial constraints in spacecraft rendezvous is maintaining the line of sight (LOS) with the target satellite, which defines a region of space moving with the target where the spacecraft must always be positioned. The cumulative mean and standard deviation of the total ΔV consumption respectively set to almost constant values, indicating that 100 simulations provide a sufficient basis to accurately assess the effectiveness of the two control strategies.

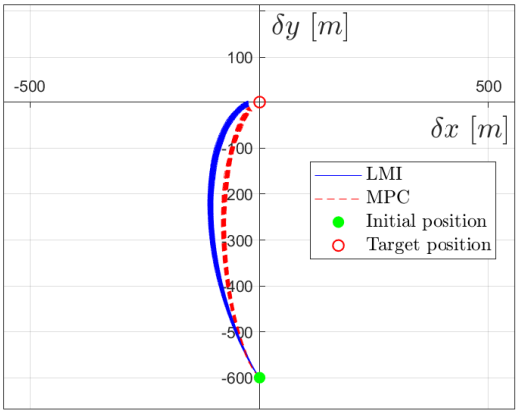

Fig. 4 Trajectories obtained through Monte Carlo analysis

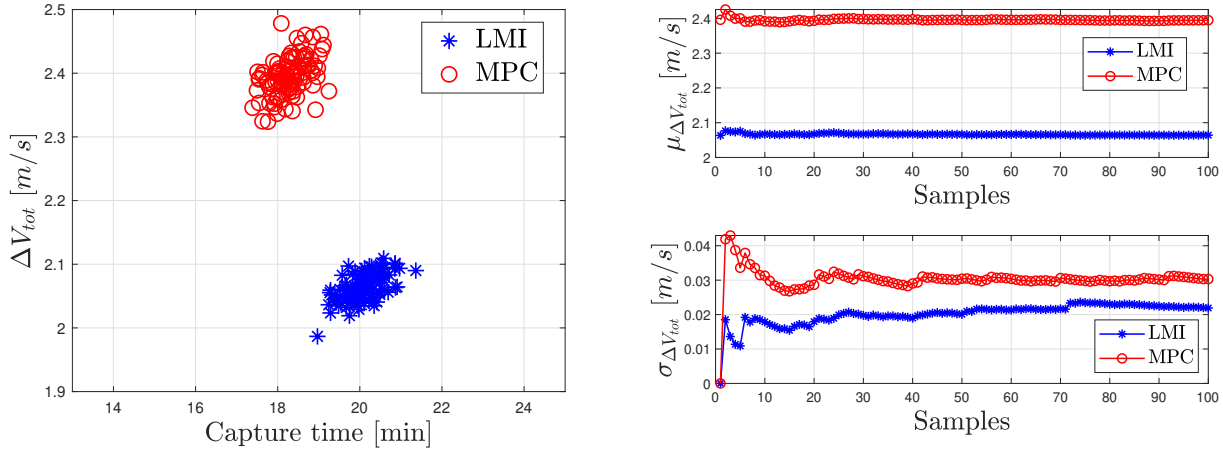

Fig. 5 Left: Consumption with respect to capture time. Right: Cumulative mean and standard deviation

4.5 Relative navigation: Kalman filter and sensor model

For the sake of a more realistic system to test and compare the developed LMI control logic, the relative navigation problem is introduced. In this scenario, the chaser spacecraft is equipped with an optical tracking camera capable of providing relative position measurements of the target, and the estimate of the full relative state $\delta\hat{\mathbf{X}}$ is obtained through an extended Kalman filter (EKF). The system encompassing the filter, sensor, and controller, is depicted in fig. 6.

The exploited measurement model of the optical tracking camera $\mathbf{y}_t = h(\delta\mathbf{X}_t, \mathbf{v}_t)$ is nonlinear, for this reason a linearization is required to use the EKF equations. It is worth noting that the measurements will only become available at specific time instants, depending on the sampling time of the sensor. Consequently, during the time intervals in which the sensor does not produce measurements, the relative state and the covariance matrix $\mathbf{P}$ are propagated through the prediction model, while when they become available, the Kalman gain is retrieved and the correction step is applied.

5 Output feedback robust hybrid control law for spacecraft rendezvous

The aim of this section is to introduce a comprehensive rendezvous manoeuvre in which both control and filter logic work together. To do so, an active space debris removal scenario is considered, where the

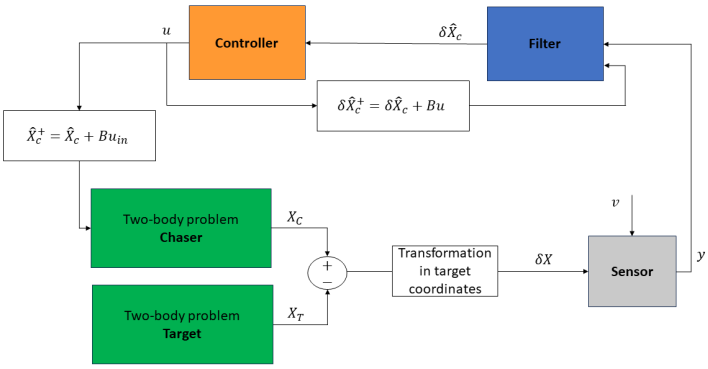

Fig. 6 System scheme: The sensor model takes the relative state δX as input and outputs the measurement vector y corrupted by noise v. The measurement is then fed into the Kalman filter that performs the prediction step, updates the Kalman gain and then corrects the estimated relative state, giving as output $\delta\hat{\mathbf{X}}_c$. Using the corrected state, the controller computes the new control input as u = K$\delta\hat{\mathbf{X}}_c$. The latter is then exploited to update the corrected estimated relative state at time t^+ (after applying the impulsive velocity change) as $\delta\hat{\mathbf{X}}_c^+ = \delta\hat{\mathbf{X}}_c$ + Bu. The new state of the chaser $\mathbf{X}_C^+$ is fed into the two-body problem as initial condition for the new integration step, where $\mathbf{u}_{in}$ represents the control action expressed in the inertial reference frame.

target object is the Envisat, a derelict spacecraft built from the European Space Agency. The Keplerian elements that define Envisat orbit (See table 1) are obtained through the TLE from 'Spacetrack.org'. Also in this case both spacecraft are positioned in the same orbit.

Table 1 Keplerian elements: Envisat

a [km]	e []	i [deg]	Ω [deg]	ω [deg]	$\theta_{0,T}$ [deg]
7142	1.3480×10^{-4}	98.2538	287.9293	85.4987	0

In this ultimate simulation, we modify the weighting factors and control parameters for both LMI and MPC controllers, aiming to gain deeper insights into their distinctive behaviors and characteristics. The results of the Monte Carlo simulations, considering 100 simulations for each case, are displayed in figs. 7 and 8 and table 2.

Table 2 Average consumption and capture time

	ΔV_{tot} [m/s]	capture time [min]
LMI - case 1	2.91	23.79
LMI - case 2	4.48	14.50
MPC - case 1	4.44	16.51
MPC - case 2	5.47	14.88
MPC - case 3	3.29	22.54

To begin with, it is important to observe that the LMI - case 2 ($\diamond$) concludes the manoeuvre at both 14 and 14.5-minute marks. This occurs because the simulation halts when the relative velocity drops below 0.2 m/s, and this state is reached during the final control action. Therefore, if the criterion is not

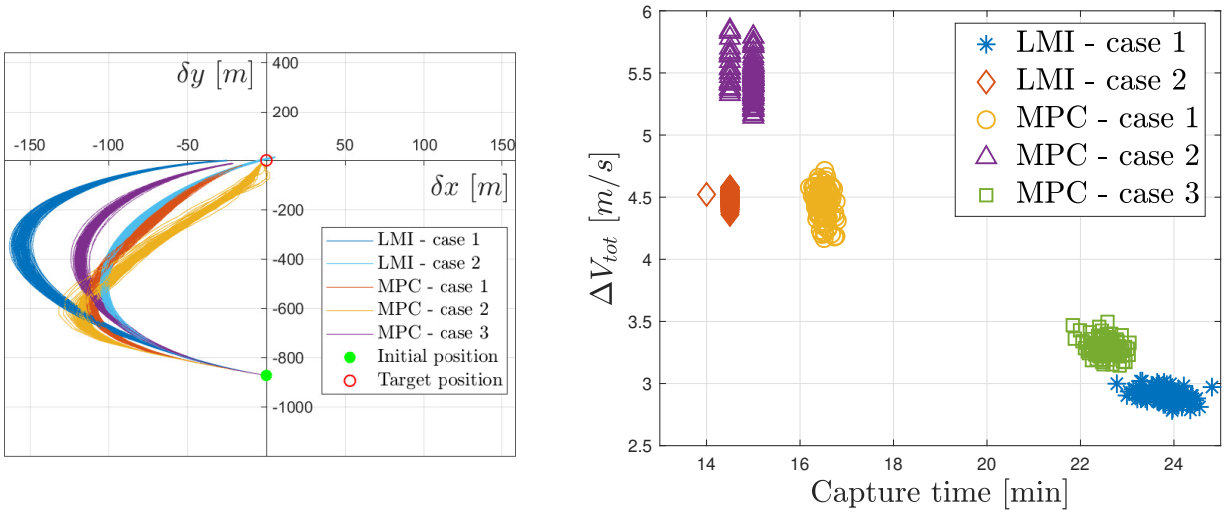

Fig. 7 Left: Trajectories obtained through Monte Carlo analysis. Right: Consumption with respect to capture time.

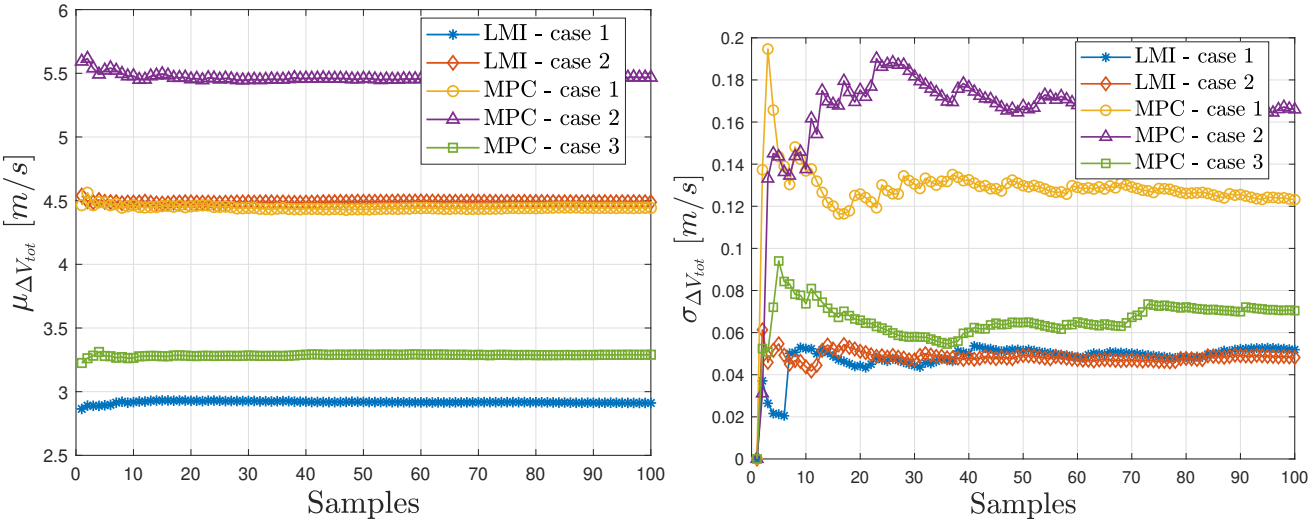

Fig. 8 Left: Cumulative mean. Right: Cumulative standard deviation

met at the 14-minute mark, an extra impulsive velocity change is applied, resulting in an additional 30 seconds to complete the rendezvous. This is a consequence of the initial high control action causing the chaser to rapidly accelerate toward the target, necessitating a swift deceleration in the last moments of the operation.

The relationship between consumption and capture time is straightforward: as capture time decreases, consumption increases, and vice versa. This is due to the greater velocity changes needed for acceleration and deceleration at both the beginning and end of the manoeuvre when considering small capture times. Comparing the total ΔV consumption between LMI - case 2 ($\diamond$) and MPC - case 1 - ($\circ$), they present similar values. However, MPC requires a longer capture time with respect to LMI. On the other hand, analyzing the LMI - case 2 ($\diamond$) and MPC - case 2 ($\triangle$), the LMI achieves an almost 18 % reduction in ΔV consumption compared to MPC.

If the total capture time of the manoeuvre is extended up to 22-23 minutes, LMI - case 1 ($*$) and MPC - case 3 ($\square$) demonstrate comparable performances. To summarize, both controllers show comparable behaviours, with a slight advantage for LMI when shorter capture times are considered.

The state estimation error is shown in fig. 9, derived from a single instance of LMI - case 1 ($*$). The initial estimation error, influencing the state estimate, can lead to undesired behaviors of the real system and potentially harm the actuators. To address this concern, the filter is engaged in the first 150 seconds

of operation with the control system inactive. This allows the filter to lock onto the true state before the control system is activated.

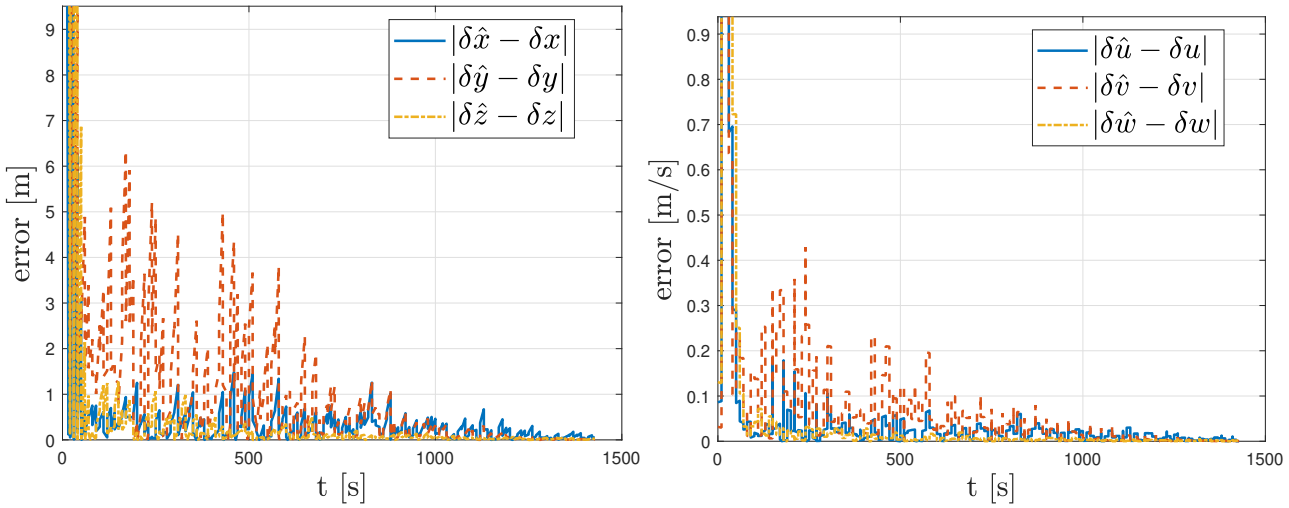

Fig. 9 Left: Estimation error of the relative position. Right: Estimation error of the relative velocity. $T_s = 30\ s$, $\phi = 0.01\ deg/pixel$, $\delta\theta_\mathbf{c}$: $\delta\bar{\theta}_\mathbf{c} = 0$,$\sqrt{\Sigma_{ii}} = 3.3 \times 10^{-4}$

6 Conclusion

The pursuit of autonomous strategies for spacecraft rendezvous holds paramount importance, driving development of new control methods to address this scenario. The design of the robust hybrid control strategy yielded excellent results, showcasing enhanced control performance against noise when compared to its non-robust counterpart. The comparison between LMI and MPC controllers through Monte Carlo analysis demonstrates that the developed control strategy is not only viable but also competitive when compared to established and tested controllers. It exhibits similar performance characteristics, affirming its efficacy in practice. Despite the utilization of the simple Hill-Clohessy-Wiltshire rendezvous model for the development of the control strategy, simulations confirm its effectiveness in scenarios where the nonlinear two-body problem model is employed to propagate spacecraft dynamics and account for disturbances. Our future efforts will be focused on enforcing safety constraints explicitly in this hybrid framework.

Acknowledgments

R. Vazquez was supported by grant TED2021-132099B-C33 funded by MICIU/ AEI/ 10.13039 /501100011033 and by "European Union NextGenerationEU/PRTR". The work of A. Seuret is supported by "European Union NextGenerationEU".

References

[1] Andreas M Hein, Robert Matheson, and Dan Fries. A techno-economic analysis of asteroid mining. *Acta Astronautica*, 168:104–115, 2020.

[2] Kwangwon Lee, Chandeok Park, and Youngho Eun. Real-time collision avoidance maneuvers for spacecraft proximity operations via discrete-time Hamilton–Jacobi theory. *Aerospace Science and Technology*, 77:688–695, 2018.

[3] Craig Underwood, Sergio Pellegrino, Vaios J Lappas, Christopher P Bridges, and John Baker. Using cubesat/micro-satellite technology to demonstrate the autonomous assembly of a reconfigurable space telescope (AAReST). *Acta Astronautica*, 114:112–122, 2015.

[4] Takahiro Sasaki, Yu Nakajima, and Toru Yamamoto. Tradeoff study for approach trajectory of active debris removal satellites considering safety, fuel consumption, and operation. In *title JAXA Special Publication: Proceedings of the 8th Space Debris Workshop*, page 461, 2019.

[5] Chris D'Souza, Chad Hannak, Pete Spehar, Fred Clark, and Mark Jackson. Orion rendezvous, proximity operations and docking design and analysis. In *AIAA guidance, navigation and control conference and exhibit*, page 6683, 2007.

[6] Michael J Neufeld. von Braun and the lunar-orbit rendezvous decision: finding a way to go to the moon. *Acta Astronautica*, 63(1-4):540–550, 2008.

[7] WH Clohessy and RS Wiltshire. Terminal guidance system for satellite rendezvous. *Journal of the aerospace sciences*, 27(9):653–658, 1960.

[8] R. Goebel, R.G. Sanfelice, and A.R. Teel. *Hybrid Dynamical Systems: modeling, stability, and robustness*. Princeton University Press, 2012.

[9] Francisco Gavilan, Rafael Vazquez, and Eduardo F. Camacho. Chance-constrained model predictive control for spacecraft rendezvous with disturbance estimation. *Control Engineering Practice*, 20(2):111–122, 2012.

[10] Julio C Sanchez, Francisco Gavilan, Rafael Vazquez, and Christophe Louembet. A flatness-based predictive controller for six-degrees of freedom spacecraft rendezvous. *Acta Astronautica*, 167:391–403, 2020.

[11] R. Vazquez, F. Gavilan, and E.F. Camacho. Pulse-width predictive control for ltv systems with application to spacecraft rendezvous. *Control Eng. Pract.*, 60:199–210, 2017.

[12] J.C. Sanchez, F. Gavilan, and R. Vazquez. Chance-constrained model predictive control for near rectilinear halo orbit spacecraft rendezvous. *Aerosp Sci Technol*, 100:105827, 2020.

[13] Mirko Brentari, Sofia Urbina, Denis Arzelier, Christophe Louembet, and Luca Zaccarian. A hybrid control framework for impulsive control of satellite rendezvous. *IEEE Transactions on Control Systems Technology*, 27(4):1537–1551, 2018.

[14] Howard D. Curtis. *Orbital Mechanics for Engineering Students*. Elsevier Butterworth-Heinemann, 2005.

[15] R. Goebel, R.G. Sanfelice, and A.R. Teel. Hybrid dynamical systems. *IEEE Control Systems*, 29(2):28–93, 2009.

[16] Mirko Brentari. *Hybrid Control For Aerospace Systems*. PhD thesis, Università degli studi di Trento, 2019.

[17] CW Scherer. LMI relaxations in robust control. *European Journal of Control*, 12(1):3–29, 2006.

[18] Tommaso Del Carro. Model predictive control for orbit and coupled attitude- orbit spacecraft rendezvous, 2022. Master Thesis, Politecnico di Milano. `https://hdl.handle.net/10589/196267`.